Measurement of the properties of the $\overline{\Omega}^+$ and Ω^- hyperons

A. W. Chan and K. C. Cheng
Institute of Physics, Academia Sinica, Taipei, Taiwan 11529, Republic Of China

K. B. Luk,* C. James, and R. Rameika
Fermilab, Batavia, Illinois 60510

P. M. Ho,† M. J. Longo, and A. Nguyen
Department of Physics, University of Michigan, Ann Arbor, Michigan 48109

J. Duryea, G. Guglielmo,‡ K. Heller, and K. Johns§
School of Physics and Astronomy, University of Minnesota, Minneapolis, Minnesota 55455

H. T. Diehl,‖ S. Teige,¶ G. B. Thomson, and Y. Zou
Department of Physics and Astronomy, Rutgers University, Piscataway, New Jersey 08854

(E756 Collaboration)
(Received 26 March 1998; published 20 August 1998)

We have analyzed $\overline{\Omega}^+$ and Ω^- events produced in the inclusive reaction $p+\mathrm{Be}\rightarrow\Omega+X$ and have measured some properties of the $\overline{\Omega}^+$ and Ω^- hyperons via the decay $\Omega\rightarrow\Lambda K\rightarrow p\pi K$. The measured $\overline{\Omega}^+$ lifetime was $\tau_{\overline{\Omega}}=(0.823\pm0.038)\times10^{-10}$ s $(\chi^2/N_{DF}=1.52)$, and the measured decay parameter was $\alpha_{\overline{\Omega}}=0.017\pm0.077$ $(\chi^2/N_{DF}=1.74)$. The corresponding values for the Ω^- were $\tau_{\Omega}=(0.817\pm0.022)\times10^{-10}$ s $(\chi^2/N_{DF}=1.17)$ and $\alpha_{\Omega}=-0.028\pm0.047$ $(\chi^2/N_{DF}=1.49)$. In addition, the measurement of the normalized mass difference between the $\overline{\Omega}^+$ and Ω^- yielded $\Delta M_{\Omega}/M_{\Omega}=(1.44\pm7.98)\times10^{-5}$. The measurements were all in good agreement with *CPT* invariance. [S0556-2821(98)02417-5]

PACS number(s): 14.20.Jn, 13.30.−a

I. INTRODUCTION

We have analyzed a sample of about 9000 $\overline{\Omega}^+$ and Ω^- events which decayed via the chain $\Omega\rightarrow\Lambda K\rightarrow p\pi K$. In this paper, we describe the analysis of these data. We report lifetime and decay parameter measurements for both $\overline{\Omega}^+$ and Ω^- and a measurement of the normalized mass difference between the $\overline{\Omega}^+$ and Ω^- hyperons.

These results are the most precise measurements of the properties of $\overline{\Omega}^+$ at present. A comparison of the $\overline{\Omega}^+$ and Ω^- properties with the statistical significance comparable to the previously best measured strange baryons, the Λ^0 and $\overline{\Lambda}^0$, is presented. Previous measurements of the $\overline{\Omega}^+$ and Ω^- properties can be found in the literature [1].

The Ω hyperon fits well into a SU(3) decuplet; so we assume it is a spin-$\frac{3}{2}$ particle. It can have $L=1,2$ for the orbital angular momentum of the final states in the weak decay $\Omega\rightarrow\Lambda K$, and the $\Omega\rightarrow\Lambda K$ matrix element is expected to be a function of the P and D waves. The $\Omega\rightarrow\Lambda K$ decay process can be partially characterized by the decay parameter

$$\alpha=2\frac{\mathrm{Re}(P^{\star}D)}{(|P|^2+|D|^2)}. \tag{1}$$

A measurement of the decay parameter α allows us to determine the degree of mixing between the parity-conserving P wave and the parity-changing D wave in the $\Omega\rightarrow\Lambda K$ decay process [2]. A dominant P wave, as predicted by theory [3], would indicate that the $\Omega\rightarrow\Lambda K$ decay proceeds primarily through the parity-conserving part of weak interactions and leads to the prediction that $\alpha_{\Omega}\simeq0$. In addition, *CP* invariance requires $\overline{\Omega}^+$ and Ω^- to have opposite sign α's ($\alpha_{\overline{\Omega}^+}=-\alpha_{\Omega^-}$).

Comparison of the lifetime and mass of the $\overline{\Omega}^+$ and Ω^- hyperons provides us with tests of *CPT* invariance, which requires the particle and antiparticle to have the same lifetime and mass. Previous results from CERN and Fermilab indicate no *CPT*-violating effect in K^0 and $\overline{K}^0$ decays [4,5].

II. EXPERIMENTAL SETUP

The experiment was performed in the Proton Center beam line at Fermilab. An 800 GeV/c proton beam incident on a

*Current address: Department of Physics, University of California, Berkeley, CA 94720.
†Current address: Lawrence Berkeley Laboratory, Berkeley, CA 94720.
‡Current address: Department of Physics and Astronomy, University of Oklahoma, Norman, OK 73019.
§Current address: Department of Physics, University of Arizona, Tucson, AZ 85721.
‖Current address: Fermilab, Batavia, IL 60510.
¶Current address: Department of Physics, Indiana University, Bloomington, IN 47405.

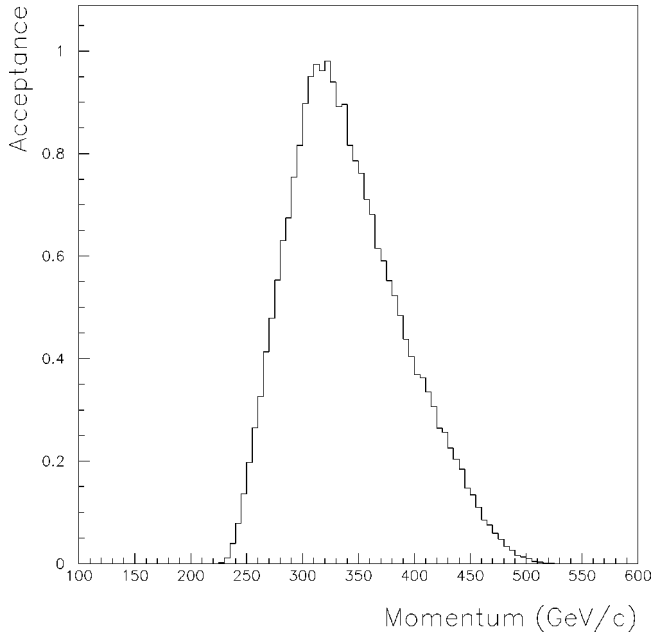

FIG. 1. Collimator acceptance for $B=2.1$ T.

beryllium target was used to create a secondary beam of particles. The secondary beam particles were charge and momentum selected by the hyperon magnet (M1) in a curved collimator and the narrowest part of the collimator (5×5 mm^2) defined the size of the secondary beam. The central orbit of the curved collimator corresponded to a 313 GeV/c particle when the magnetic field was set to $B=2.1$ T. The acceptance distribution for $B=2.1$ T (see Fig. 1) was calculated via Monte Carlo simulation and was defined as the ratio of the number of charged particles in the secondary beam exiting the collimator to the number entering the collimator for each momentum bin.

The spectrometer was made up of eight silicon strip detectors (SSD1–8), five scintillation counters (S1, S2, V1, V2 and M), nine multiwire proportional chambers (C1–C9), and an analyzing magnet (M2), as shown in Fig. 2. The coordinate system was defined with the z axis along the centerline of the charged beam as it emerged from M1. The y axis was vertically upward, and the x axis was horizontal.

The eight SSD planes were divided into four x planes and four y planes. These were installed downstream of the M1 exit and were used to detect secondary beam particles.

The scintillation counters S1 and S2 served as beam counters. V1 and V2 were veto counters surrounding S1 and S2; their function was to eliminate beam particles accompanied by a charged halo. The pulse height of the M counter was proportional to the number of minimum ionizing particles (m.i.p.'s) which passed through it simultaneously.

Chambers C1–C9 had vertical (x-view) and horizontal (y-view) wire planes, except for C5 which had two orthogonal wire planes rotated 45° about the z axis. C1–C3 had 1 mm wire spacing, and C4–C9 had 2 mm wire spacing. In addition, C6 had a third wire plane with 2.8 mm wire spacing, rotated 45° about the z axis. These rotated planes were used for associating multiple hits in the x and y views during event reconstruction.

The M2 analyzing magnet had an upstream aperture of 61×25 cm^2 and a downstream aperture of 61×30 cm^2. The magnetic field could point either in the $+$y or $-$y direction with a transverse momentum kick of 1.54 GeV/c in the x-z plane. The components of the magnetic field were measured with a moving coil on a 2.54 cm grid, and the consistency of the magnetic field strength was checked at the 1% level by comparing the reconstructed Ξ^- mass with the accepted value.

When the polarity of M1 was set to select a negative secondary beam, the beam was composed of a mixture of π^-, K^-, Σ^-, Ξ^-, Ω^-, and $\bar{p}$. A secondary beam with opposite charge was selected by reversing the polarity of M1. The particles and antiparticles were detected under similar conditions, except for the polarity of M1 and M2. This was useful in cross-checking physical measurements and analysis programs in the experiment.

For this analysis, data were taken with the hyperon magnet (M1) set to an average field of 2.1 T, corresponding to secondary beam momentum of 230–520 GeV/c. The wide momentum acceptance of the collimator is shown in Fig. 1.

For the negative secondary beam runs, the magnetic fields of both M1 and M2 were pointed in the $-$y direction. The decay sequence of interest in this case was $\Omega^-\to\Lambda K^-\to p\pi^-K^-$. After M2, protons were bent to the $+$x direction, and the π^- and K^- were bent to the $-$x direction. The trigger was designed to reject high-multiplicity events, such

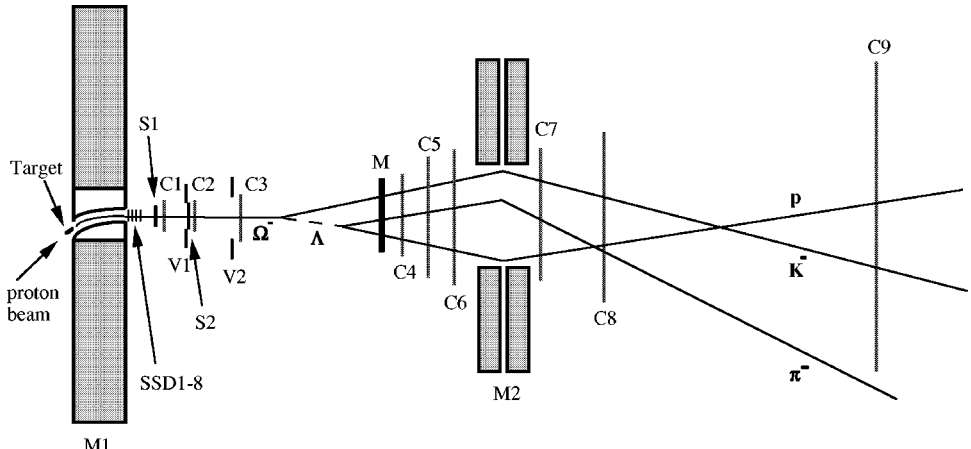

FIG. 2. Plan view of the E756 spectrometer (not to scale).

as those originating from secondary beam interactions with the collimator walls, and single track events (high-momentum single pions, for example). Therefore, the trigger required a signal from S1 and S2 with no signal from V1 and V2, and the pulse height from the multiplicity counter M was required to correspond to more than two but less than five m.i.p.'s. The trigger also required at least one hit on the right side of C8 ($-$x) and at least one hit on the left side of C9 ($+$x). An event was accepted if the signals from all scintillation counters and chambers satisfied the above requirements. For the positive secondary beam runs, the magnetic fields of M1 and M2 were reversed, and the same trigger requirements were applied.

The efficiencies of the detectors were monitored regularly with single track events. For the entire run, the average efficiencies of the SSD's and C1–C9 were roughly 84.3% and 93.4%, respectively.

III. MONTE CARLO SIMULATION

A Monte Carlo program was written to simulate the experiment as closely as possible. It was used for determining the acceptance, the resolution of the spectrometer, the efficiency of the event reconstruction program, and the possible backgrounds to the Ω samples.

In the Monte Carlo program, Ω^- particles were generated at the target with a specified initial momentum and required to pass through the collimator. In the fiducial region, the Ω^- particles were decayed without any polarization into Λ and K^- and followed an exponential distribution with a specified input lifetime and input decay parameter α_Ω. The lifetime and decay parameter could be varied if needed. The daughter Λ was then decayed into p and π^- with a longitudinal polarization related to α_Ω. The lifetime and decay parameter of the Λ were fixed at the accepted values [1].

The charged particles in the decay were traced through the software aperture of the spectrometer. Multiple scattering effects, proportional to the amount of material in the spectrometer and with Molière tail, were incorporated in the tracing process. A single-bend plane approximation of the M2 magnetic field was used to simulate the passage of the charged particles through M2. Small inhomogeneity and time-variation effects in the magnetic field of M2, as determined from the map of the magnetic field and actual running conditions, were also simulated.

If the event satisfied the software trigger requirements, the spatial positions of the charged particles at each silicon strip detector and multiwire proportional chamber were digitized into wire hits. Care was taken to ensure that each detector was given the proper hit multiplicity, the correct resolution, and correct efficiency, as seen in the data.

The wire hits were then reconstructed with the same reconstruction program used on the data. Finally, the reconstructed Monte Carlo events were required to satisfy the same set of selection cuts (see Sec. IV) as the data, before they were utilized for physics analyses.

IV. EVENT SELECTION

The reconstruction program was designed to search for events with a three-track, two-vertex topology (such as $\Omega \to \Lambda K \to p\pi K$). A detailed description of the reconstruction algorithm can be found elsewhere [6,7]. This initial filtering process removed most background events with the wrong topology, but a significant portion of background events with the desired topology passed the initial filtering process. These background events consisted mostly of $\Xi \to \Lambda\pi$ and $\Omega \to \Xi^0\pi$. Therefore, we required additional cuts to reduce the background.

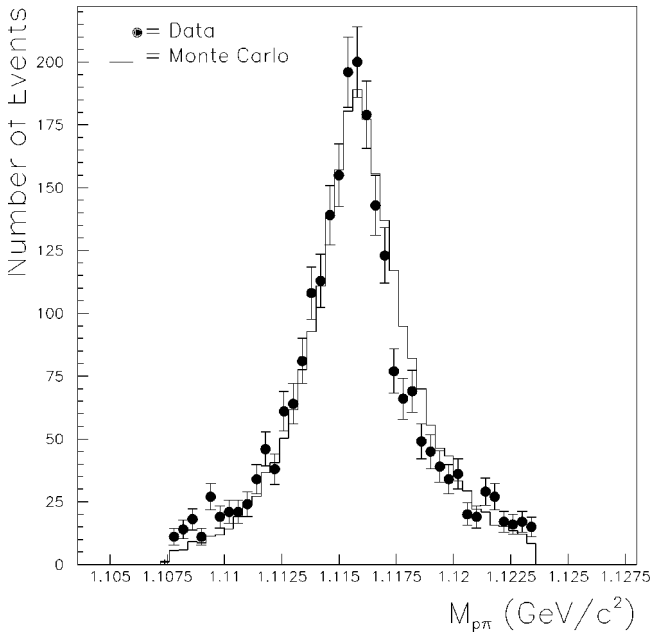

FIG. 3. The $M_{p\pi}$ distribution for the $\overline{\Omega}^+$ sample after applying all event selection cuts except for the $M_{\Lambda K}$ cut.

(a) *Cut on χ^2 of geometric fit*. The geometric fit χ^2 measured the quality of the fit of the three tracks to the desired topology (two decay vertices and three daughter tracks). We required $\chi^2 < 100$ (for typically 32 degrees of freedom) in order to accept the candidate event. Further details about the geometric fit χ^2 cut can be found elsewhere [6,7].

(b) *Cut on $p\pi$ invariant mass*. Since a Λ must be present in the decay chain, the reconstructed $p\pi$ invariant mass $M_{p\pi}$ was restricted to the range 1.1075–1.1235 GeV/c^2, as shown in Fig. 3.

(c) *Cut on $\Lambda\pi$ invariant mass*. The three-track, two-vertex event sample was dominated by $\Xi \to \Lambda\pi$ events, and the reconstruction did not distinguish the π from the K in the similar $\Omega \to \Lambda K$ decay. Using the $\Lambda\pi$ mass hypothesis, we required $M_{\Lambda\pi} > 1.345$ GeV/c^2, which is 24 MeV/c^2 (10σ) higher than $M_\Xi = 1.321$ GeV/c^2.

(d) *Cut on 3π invariant mass*. Because of the finite position resolution of the spectrometer, the fitting code sometimes reconstructed two vertices for $K^\pm \to 3\pi$ events which decayed inside the decay volume. Therefore, in order to remove K from our sample, we used the 3π mass hypothesis and eliminated all events with invariant mass $M_{3\pi} < 0.510$ GeV/c^2.

(e) *Cut on the z position of the decay vertices*. The reconstructed z distribution of the vertices indicated that the secondary beam interactions with the multiplicity counter (z

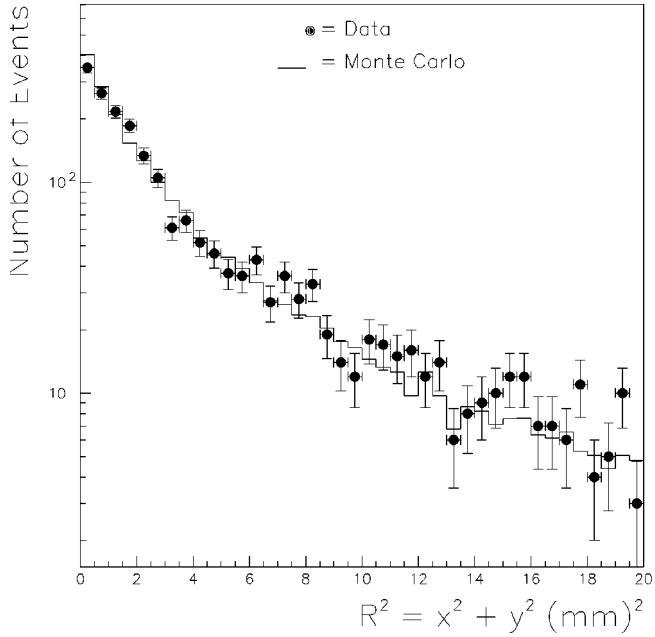

FIG. 4. The distribution for the $R^2=x^2+y^2$ variable for the $\overline{\Omega}^+$ sample after applying all cuts.

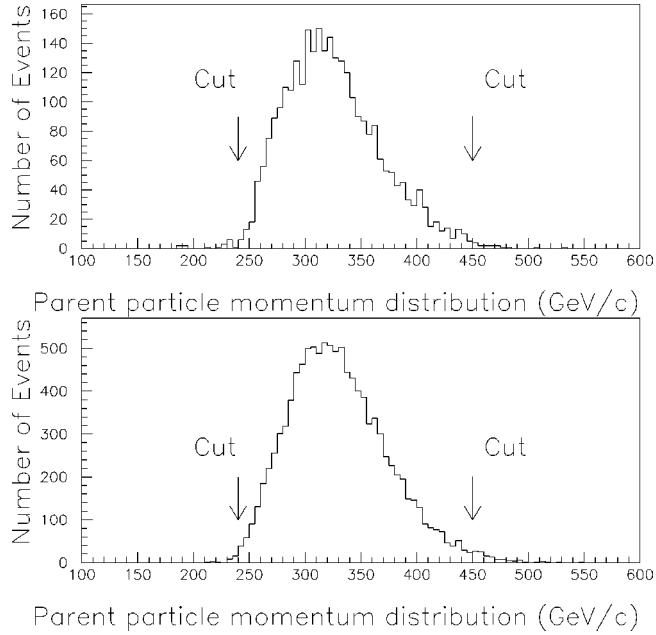

FIG. 5. The momentum distribution before applying the momentum cuts for $\overline{\Omega}^+$ (top) and Ω^- (bottom) candidate events.

$=2300$ cm) created background events in that region. These background events consisted of secondary beam particles scattered in the M counter to produce three-track events that were occasionally reconstructed poorly as decay products of Ω hyperons. In addition, secondary beam particles which decayed inside the collimator, with the decayed particles clearing the channel, were another potential source of background events near $z=0$ cm. Therefore, we required the z position of the two vertices to lie in the range $75<z<2300$ cm.

(f) *Cut on the target-pointing variable*. The reconstructed momentum of the parent particle ($\overline{\Omega}^+$ or Ω^-) was traced back through the hyperon magnet using the measured magnetic field value to the location of the production target. The projected position was required to be within $R^2=x^2+y^2<20$ mm^2 of the target center (see Fig. 4). We required that the parent particle originate from the target in order to reduce background from events produced inside the collimator or from secondary beam interactions with material in the spectrometer. This cut was based on detailed measurements of the spread of the incoming proton beam at the target [6,7].

(g) *Cut on momentum*. Based on the channel acceptance, the momentum range of the Ω hyperon was approximately 230–500 GeV/c. Events with reconstructed parent momenta beyond this range might be due to misreconstruction. To minimize background we restricted the momentum range for candidate events to 240–450 GeV/c. Figure 5 shows the momentum distributions of candidate events for both $\overline{\Omega}^+$ and Ω^- before the momentum cut.

(h) *Angular cut in $\Lambda\pi$ center of mass frame*. To further reduce $\Omega\rightarrow\Xi^0\pi$ background, we computed the angle θ_Λ between the Λ momentum and the z axis in the $\Lambda\pi$ center of mass frame. It was found that the $\Omega\rightarrow\Lambda K$ events were restricted to $\cos\theta_\Lambda<-0.4$, as shown in Fig. 6, while the $\Omega\rightarrow\Xi^0\pi$ events covered the full range in $\cos\theta_\Lambda$. Therefore, a cut requiring $\cos\theta_\Lambda<-0.4$ was made.

(i) *Decay angle cuts in ΛK center of mass frame*. To further reduce background events, we computed the angles θ_K and ϕ_K in the ΛK center of mass frame. The angle θ_K was defined as the angle between the K momentum and the z axis, and the ϕ_K angle was the azimuthal angle of the K momentum in the x-y plane. Monte Carlo studies of $\Xi\rightarrow\Lambda\pi$ events showed that most of these events appear to the

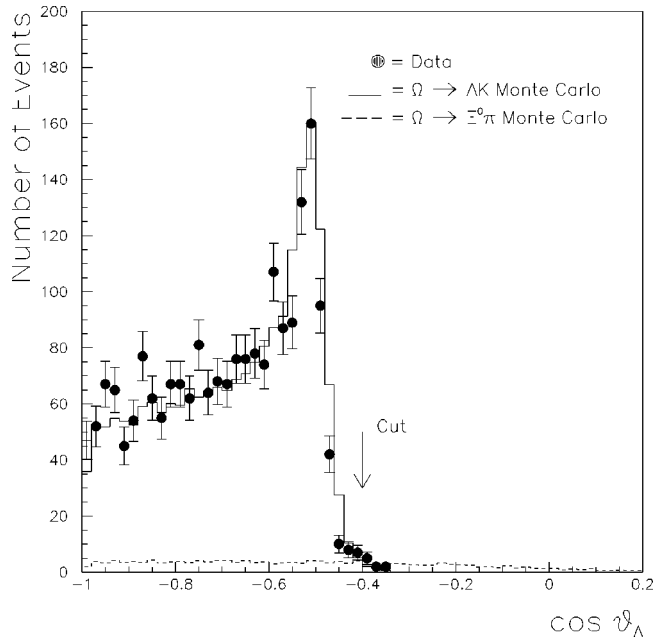

FIG. 6. The $\cos\theta_\Lambda$ distribution for the $\overline{\Omega}^+$ sample before applying the $\cos\theta_\Lambda$ cut.

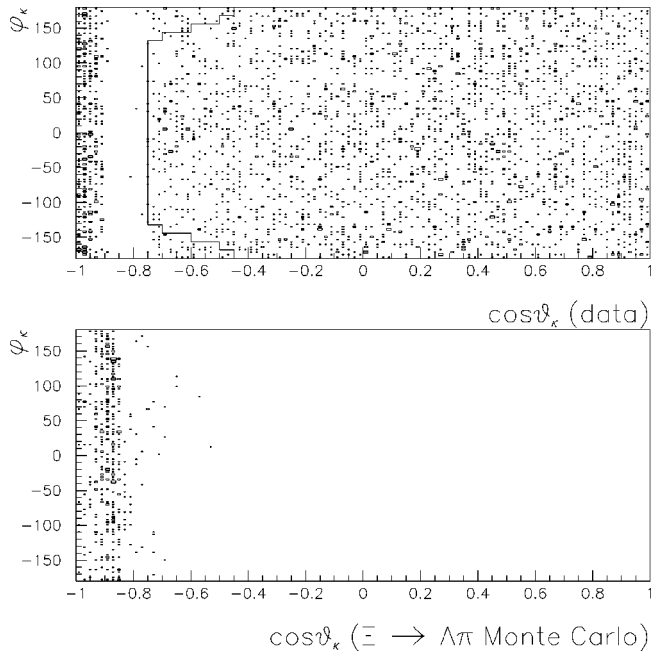

FIG. 7. The cos θ_K vs ϕ_K distribution of the K in the ΛK center of mass frame ($\overline{\Omega}^+$ sample) before applying the decay angle contour cut. Data events to the left of the contour line were rejected.

left of a contour line in the cos θ_K vs ϕ_K scatter plot, as shown in Fig. 7(b).

(j) *Cut on ΛK invariant mass*. We made one final cut, by requiring that $1.657 < M_{\Lambda K} < 1.687$ GeV/c^2 (see Fig. 8).

Monte Carlo studies showed that the selection efficiency for $\overline{\Omega}^+$ (Ω^-) was 48.6% (49.7%). The amount of background was estimated by fitting the mass distribution for $\overline{\Omega}^+$ (Fig. 8) and Ω^- candidate events in the range of

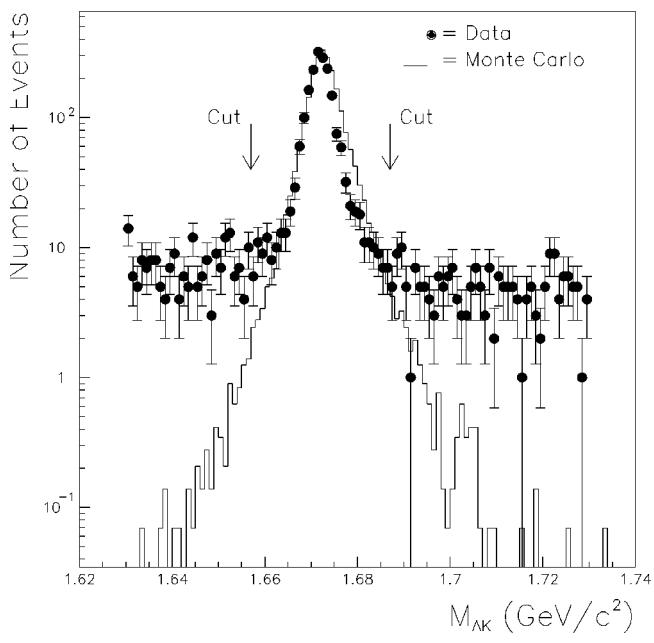

FIG. 8. The ΛK invariant mass distribution for the $\overline{\Omega}^+$ sample before applying the $M_{\Lambda K}$ cut.

1.657 GeV/$c^2 < M_{\Lambda K} < 1.687$ GeV/c^2 with a combination of a Gaussian and a linear function. The background rate was estimated from the linear part of the fit to be 3.7% (3.6%) for $\overline{\Omega}^+$ (Ω^-). Monte Carlo studies indicated that roughly 59% of this background was due to $\Omega \rightarrow \Xi^0\pi$ events, and the remainder was mostly due to $\Xi \rightarrow \Lambda\pi$ events. Tables I and II summarize the results of the event selection.

The Monte Carlo simulation program was verified with data containing single track events, data taken at different targeting angles (including zero targeting angle), different magnetic fields for M1, and different data samples ($\overline{\Xi}^+$, Ξ^-, and $K^\pm$). We compared various distributions, including geometric χ^2 distribution, decay vertices distributions, momentum spectra of various particles, and $p\pi$ and ΛK mass distributions. In all cases data and Monte Carlo simulations were in good agreement [7].

V. ANALYSIS

Three analyses were performed: lifetime, decay parameter, and mass difference. The lifetime and decay parameter analyses were done for both $\overline{\Omega}^+$ and Ω^-, and the mass difference analysis was done by comparing the measured $\overline{\Omega}^+$ and Ω^- masses.

A. Lifetime

The decay of an unstable particle in flight can be described by an exponential distribution

$$N(z) = N(0)e^{-(mz/p\tau)}, \tag{2}$$

where $N(z)$ is the number of surviving particles at a distance z from a given reference point ($z=0$), and m, p, and τ are the mass, momentum, and lifetime of the particle, respectively. In reality, beams of particles are produced with a range of momenta and detected by devices with imperfect acceptance. Therefore, Eq. (2) was modified to represent the observed distribution

$$N(p,z) = \epsilon(p,z)N(p,z_0)e^{-(mz/p\tau)}, \tag{3}$$

where the detector acceptance $\epsilon(p,z)$ was determined by Monte Carlo calculation. A reference point 75 cm downstream of the exit of M1 ($z_0 = 75$ cm) was used [see Fig. 2 and cut (e) in Sec. III].

Four independent (different initial random number seeds) Monte Carlo samples, one with $c\tau_0 = 2.06$ cm, two with $c\tau_0 = 2.46$ cm, and another with $c\tau_0 = 2.86$ cm, were generated for the lifetime analyses, corresponding to input Ω lifetimes ranging from $\tau_0 = 0.68 \times 10^{-10}$ to 0.95×10^{-10} s. Each generated sample contained 100 000 events. The Λ lifetime was fixed at the accepted value ($\tau_\Lambda = 2.632 \times 10^{-10}$ s) [1]. The Monte Carlo events were generated with a momentum spectrum similar to that of data events at the exit of M1. The Ω decay spectrum of the generated events followed the exponential distribution

$$N(\tau_0,p,z) = \epsilon(p,z)N(p,z_0)e^{-(mz/p\tau_0)}. \tag{4}$$

TABLE I. Summary of event selection cuts for Ω^-. The first column shows the various selection cuts used in the Ω event selection. The second column shows the number of Ω^- data events passing each selection cut. The remaining four columns show the percentage of each type of Monte Carlo (MC) event passing each selection cut, where ''Other'' represents the statistical sum of $K^- \to 3\pi$ and $\Omega^- \to \Xi^- \pi^0$ Monte Carlo events. The cuts were applied sequentially.

Cut	Data	% of MC events left			
		$\Omega^- \to \Lambda K^-$	$\Omega^- \to \Xi^0 \pi^-$	$\Xi^- \to \Lambda \pi^-$	Other
Before cuts	76878	100.0	100.0	100.0	100.0
Geometric χ^2	76843	99.8	99.8	99.7	99.6
$M_{p\pi}$	49936	90.4	92.6	89.0	44.8
$M_{\Lambda\pi}$	26743	78.5	92.1	2.0	0.9
$M_{3\pi}$	26636	78.4	92.0	2.0	0.8
Z vertex	13349	61.3	64.2	1.6	0.1
Target	8619	55.6	13.3	0.5	0.04
Momentum	8296	52.0	12.5	0.2	0.02
$\cos\theta_\Lambda$	8034	51.9	7.9	0.03	0.003
θ_K, ϕ_K	7618	50.4	7.9	0.02	0.003
$M_{\Lambda K}$	6953	49.7	3.3	0.01	0.003
Est. No. of events					
Before cuts		67915	22264	4991294	83358
After cuts		33771	727	499	3

TABLE II. Summary of event selection cuts for $\overline{\Omega}^+$. The first column shows the various selection cuts used in the Ω event selection. The second column shows the number of $\overline{\Omega}^+$ data events passing each selection cut. The remaining four columns show the percentage of each type of Monte Carlo event passing each selection cut, where ''Other'' represents the statistical sum of $K^+ \to 3\pi$ and $\overline{\Omega}^+ \to \overline{\Xi}^+ \pi^0$ Monte Carlo events. The cuts were applied sequentially.

Cut	Data	% of MC events left			
		$\overline{\Omega}^+ \to \overline{\Lambda} K^+$	$\overline{\Omega}^+ \to \overline{\Xi}^0 \pi^+$	$\overline{\Xi}^+ \to \overline{\Lambda} \pi^+$	Other
Before cuts	30391	100.0	100.0	100.0	100.0
Geometric χ^2	30376	99.8	99.9	99.7	99.5
$M_{p\pi}$	17639	90.1	92.4	88.8	44.7
$M_{\Lambda\pi}$	13370	78.2	92.2	2.0	0.8
$M_{3\pi}$	12661	78.1	92.0	1.9	0.6
Z vertex	7354	59.9	64.3	1.4	0.1
Target	2470	54.3	13.6	0.4	0.03
Momentum	2411	50.7	12.4	0.1	0.02
$\cos\theta_\Lambda$	2366	50.6	7.8	0.02	0.002
θ_K, ϕ_K	2270	49.2	7.8	0.01	0.002
$M_{\Lambda K}$	1823	48.6	3.2	0.01	0.002
Est. No. of events					
Before cuts		67487	22205	4978833	82858
After cuts		32793	703	492	2

The data and Monte Carlo events were subjected to the same reconstruction code and event selection (see sec. III). Furthermore, the lifetime analysis was restricted to the region 0.75 m$\leqslant z \leqslant$18 m, where the Monte Carlo simulation did a good job in reproducing the Ω z-vertex spectrum of the data. The final data samples for the lifetime analysis contained 1801 $\overline{\Omega}^+$ and 6934 Ω^- events.

We used the Monte Carlo program to define the normalization factors

$$C(p)=\frac{N_R(p)}{N_{MC}(p)}, \tag{5}$$

where the $C(p)$ are determined by the fit. The $C(p)$ factors reconcile both the differences in the shape of the momentum spectrum and the much larger size of the Monte Carlo sample. The other free parameter is $c\tau$, where c is the velocity of light. We collected data and Monte Carlo events into 5 GeV/c momentum bins and 0.5 m decay vertex position bins. For simplicity, we introduce the following notation: $r_{ij}=N_R(p_i,z_j)$ and $m_{ij}=N_{MC}(p_i,z_j)$.

Because of low statistics, the population of bins far away from the origin ($z\gtrsim 10$ m) was not very high, and so a least-squares minimization of χ^2 (which assumes a Gaussian distribution of errors) was not appropriate. Therefore, we used a maximum-likelihood method with Poisson statistics. We used the Monte Carlo distribution to estimate the expected population of each bin,

$$u_{ij}=m_{ij}C_i\frac{e^{-(z_j m/p_i\tau)}}{e^{-(z_j m/p_i\tau_0)}}, \tag{6}$$

where C_i and τ are parameters to be determined in the fit. In any given bin the observed number of events, r_{ij}, occurs with a probability given by

$$\mathrm{P}_{ij}=\frac{(u_{ij})^{r_{ij}}}{r_{ij}!}e^{-u_{ij}}. \tag{7}$$

We can then write the likelihood function as the product over all momentum and z-vertex bins of these Poisson probabilities,

$$L'(C_i,\tau)=\prod_{ij}(\mathrm{P}_{ij}), \tag{8}$$

which we can rewrite as

$$L(C_i,\tau)=-2\ln(L')=-2\sum_{ij}[\ln(\mathrm{P}_{ij})]$$
$$=-2\left[\sum_{ij}r_{ij}\ln(u_{ij})-\sum_{ij}u_{ij}\right]+\text{const.} \tag{9}$$

By minimizing this logarithmic likelihood function, we obtained the Ω lifetime that yielded the most likely match between the data and Monte Carlo spectra.

Our measured lifetime corresponding to the best fit for $\overline{\Omega}^+$ is $\tau_{\overline{\Omega}}=(0.823\pm0.031)\times10^{-10}$ s, and the corresponding result for Ω^- is $\tau_\Omega=(0.817\pm0.013)\times10^{-10}$ s, where the uncertainties are statistical only. Figure 9 shows the result of the final fits for $\overline{\Omega}^+$ ($\chi^2/N_{DF}=1.52$) and Ω^- ($\chi^2/N_{DF}=1.17$), which were obtained with sample No. 3.

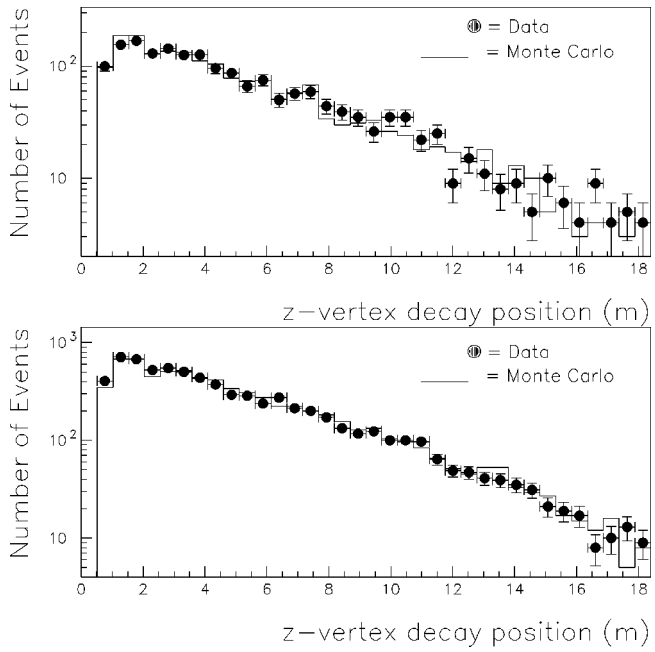

FIG. 9. The Monte Carlo ($c\tau=2.46$ cm) fit to the $\overline{\Omega}^+$ (top) and Ω^- (bottom) reconstructed decay vertices. The Monte Carlo distributions correspond to the measured lifetime yielding the best fits. The $\chi^2/33N_{DF}$ of the fits is 1.52 for $\overline{\Omega}^+$ and 1.17 for Ω^-.

We studied the stability of the lifetime fits as a function of background in two different ways. First, the momentum, z-vertex, and $M_{\Lambda K}$ cuts in the event selection process were varied in such a way that the number of events in the final sample changed by about $\simeq\sqrt{N}$, where N is the total number of selected events in the sample (1801 for $\overline{\Omega}^+$ and 6934 for Ω^-). This accounted for most of the systematic uncertainty in the analyses. In addition, Monte Carlo background events were generated, reconstructed, and passed through the event selection process (see Tables I and II). The background events surviving the selection cuts were added to the signal Monte Carlo events, and this modified Monte Carlo spectrum was fit to data. The result of this fit was compared to the nominal (signal) Monte Carlo fit result. The effect was negligible compared to the other sources of systematic uncertainties.

Fluctuations in the magnetic field of M2 directly affect the lifetime measurement since it causes the reconstruction code to miscalculate the track momentum. We estimated the uncertainty in the lifetime due to fluctuations in the M2 field by varying the nominal M2 magnetic field in the Monte Carlo simulation by 0.25%, which was the average level of fluctuation about the nominal M2 magnetic field during the data acquisition period. The systematic uncertainty due to magnetic field fluctuations in M2 was small compared to other sources of systematic uncertainties.

The bin widths were doubled to check the sensitivity of

TABLE III. Lifetime measurements.

Sample No.	$c\tau_0$ (cm)	N_{MC}	$\tau_{\bar{\Omega}}$ ($\times 10^{-10}$ s)	τ_{Ω} ($\times 10^{-10}$ s)
1	2.06	37320	0.814 ± 0.030	0.812 ± 0.013
2	2.46	37433	0.809 ± 0.031	0.818 ± 0.013
3	2.46	37480	0.823 ± 0.031	0.817 ± 0.013
4	2.86	37591	0.810 ± 0.030	0.821 ± 0.014

the lifetime fits with respect to the momentum and z resolution. We also checked the sensitivity with respect to the size of the Monte Carlo sample by dividing it into three subsamples with roughly equal statistics and redoing the analysis for each subsample. No significant systematic effect was observed in either case.

The $\bar{\Omega}^+$ momentum spectrum ($\bar{p} = 325.0$ GeV/c) was ''softer'' than the Ω^- spectrum ($\bar{p} = 329.9$ GeV/c), and so we studied the stability of the lifetime fits as a function of the reconstructed Ω momentum. Each data sample was divided into three momentum bins (240–300, 300–330, and 330–450 GeV/c^2) with roughly the same number of events in each bin, and the analysis was redone for each bin. The results produced a spread of about 0.5 standard deviations when compared to the full sample.

In addition, we checked the stability of the lifetime fits with respect to changes in the allowed decay fiducial by varying the range covered by the fitting code. The upstream boundary was varied from 0.5 to 1.5 m, and the downstream boundary was varied from 16 to 23 m. The fits yielded results within 0.5 standard deviations on the average for both $\bar{\Omega}^+$ and Ω^-.

The effect of the uncertainty in the Λ lifetime on the Ω lifetime measurement was also studied. Monte Carlo events were generated with the Λ lifetime offset by one standard deviation [1], and the Ω lifetime fits were redone with these Monte Carlo events. The results produced a spread within 0.3 standard deviations for $\bar{\Omega}^+$ and 0.4 standard deviations for Ω^- when compared with the nominal fits. The systematic effect due to the uncertainty in the Λ lifetime was estimated by comparing these lifetime fits with the fits obtained with the Λ lifetime fixed at the accepted value [1].

We also checked the measured lifetime as a function of our choice of Monte Carlo sample. The fits with the independent Monte Carlo samples yielded $c\tau$ within a standard deviation of each other for $\bar{\Omega}^+$ and Ω^-. Table III shows the results of the fits of various Monte Carlo samples to the data. The systematic effect due to the choice of Monte Carlo sample was estimated from the variation of the fit results for various Monte Carlo samples. Table IV lists the major systematic uncertainties in our analyses, which were estimated with sample No. 4.

The final result for $\bar{\Omega}^+$ is $\tau_{\bar{\Omega}} = [0.823 \pm 0.031(\text{stat}) \pm 0.022(\text{syst})] \times 10^{-10}$ s, and the corresponding result for Ω^- is $\tau_{\Omega} = [0.817 \pm 0.013(\text{stat}) \pm 0.018(\text{syst})] \times 10^{-10}$ s. By combining the statistical and systematic uncertainties in quadrature, we obtain

TABLE IV. Systematic uncertainties for lifetime measurements.

Systematic	$\tau_{\bar{\Omega}}$ ($\times 10^{-10}$ s)	τ_{Ω} ($\times 10^{-10}$ s)
Event selection	0.017	0.009
M2 field	0.002	0.008
Bin width	0.003	0.002
MC statistics	0.003	0.006
Momentum	0.009	0.006
Decay position	0.002	0.004
Lambda lifetime	0.006	0.006
MC sample	0.007	0.008

$$\tau_{\bar{\Omega}} = (0.823 \pm 0.038) \times 10^{-10} \text{ s},$$

$$\tau_{\Omega} = (0.817 \pm 0.022) \times 10^{-10} \text{ s}.$$

B. Decay parameter

In the decay $\Omega \to \Lambda K \to p\pi$, the angular distribution of the final state proton in the Λ rest frame is given by

$$\frac{dN}{d\Omega_p} = \frac{1}{4\pi}(1 + \alpha_\Lambda \vec{P}_\Lambda \cdot \hat{p}), \tag{10}$$

where Ω_p and $\hat{p}$ are the solid angle and momentum unit vector of the proton in the Λ rest frame, and α_Λ is the parameter that describes the degree of mixing of parities in the decay [2]. Since the distribution is independent of the azimuthal angle, the above expression can be rewritten as

$$\frac{dN}{d(\cos\theta)} = \frac{1}{2}[1 + \alpha_\Lambda(\vec{P}_\Lambda \cdot \hat{n})\cos\theta], \tag{11}$$

where $\hat{n}$ is an arbitrarily chosen unit vector and $\cos\theta = \hat{n} \cdot \hat{p}$, the direction cosine of the proton in the Λ rest frame.

Our data were produced at nonzero targeting angles (± 2.5 mrad), but any nonzero Ω polarization averaged to zero because there were roughly an equal number of events produced at positive and negative targeting angles [6,7]. Therefore, the Λ polarization from the Ω decay is simply

$$\vec{P}_\Lambda = \alpha_\Omega \hat{p}_\Lambda, \tag{12}$$

where $\hat{p}_\Lambda$ is the unit vector of the Λ momentum in the Ω rest frame. If we choose $\hat{n} = \hat{p}_\Lambda$, Eq. (11) becomes

$$\frac{dN}{d(\cos\theta)} = \frac{1}{2}(1 + \alpha_\Lambda \alpha_\Omega \cos\theta), \tag{13}$$

where θ is now the angle between the daughter proton momentum in the Λ rest frame and $\hat{p}_\Lambda$ (see Fig. 10).

Ten independent (different initial random number seeds) Monte Carlo samples were generated with input α_Ω ranging from -0.156 to 0.156, while α_Λ was fixed at the accepted value ($\alpha_\Lambda = 0.642$) [1]. Each generated sample contained 100 000 events. The Monte Carlo events were generated with a momentum spectrum similar to that of data events at

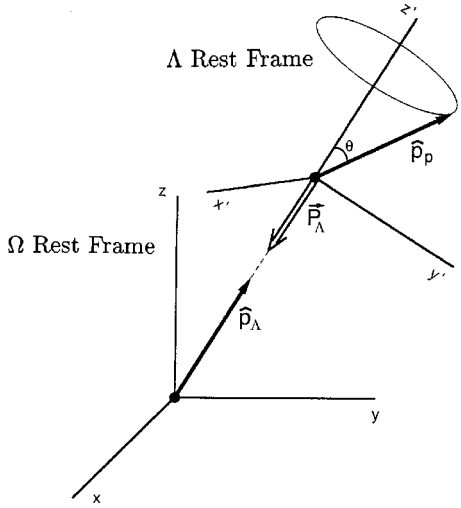

FIG. 10. Λ momentum direction defines the polar axis z' in the frame in which the cos θ distribution is measured.

the exit of M1. The angular distribution of the generated events followed the distribution shown in Eq. (13).

The data and Monte Carlo events were subjected to the same reconstruction code and event selection (see Sec. III). The final data samples contained 1823 $\overline{\Omega}^+$ events and 6953 Ω^- events.

Equation (13) was modified by the detector acceptance and reconstruction efficiency. We used the Monte Carlo program to produce a correction function for the detector acceptance and event reconstruction efficiency,

$$C(\cos\,\theta)=\frac{N_{MC}^{gen}(\cos\,\theta)}{N_{MC}^{rec}(\cos\,\theta)}\frac{N_{MC}^{rec}}{N_{MC}^{gen}}, \tag{14}$$

where $N_{MC}^{gen}(\cos\,\theta)$ and $N_{MC}^{rec}(\cos\,\theta)$ are the number of generated and reconstructed Monte Carlo events for each cos θ bin, respectively. N_{MC}^{gen} and N_{MC}^{rec} are the total number of generated and reconstructed Monte Carlo events, respectively. The modified proton distribution function is

$$\frac{dN}{d(\cos\,\theta)}=\frac{C(\cos\,\theta)}{2}(1+\alpha_\Lambda\alpha_\Omega\cos\,\theta), \tag{15}$$

where α_Ω is a parameter to be determined by the fit.

Real and Monte Carlo events were collected into cos θ bins. We use the following notation for simplicity: $a_i=dN_R/d(\cos\,\theta_i)$ and $b_i=dN_{MC}/d(\cos\,\theta_i)$, where $dN_R/d(\cos\,\theta_i)$ and $dN_{MC}/d(\cos\,\theta_i)$ are the number of events in the ith cos θ bin for real data and Monte Carlo events, respectively.

A maximum-likelihood calculation with Poisson statistics was used, and the likelihood function $L(C_i,\alpha_\Omega)$ was built, where

$$L(C_i,\alpha_\Omega)=-\sum_i a_i ln[b_i]+\sum_i b_i+\text{const.} \tag{16}$$

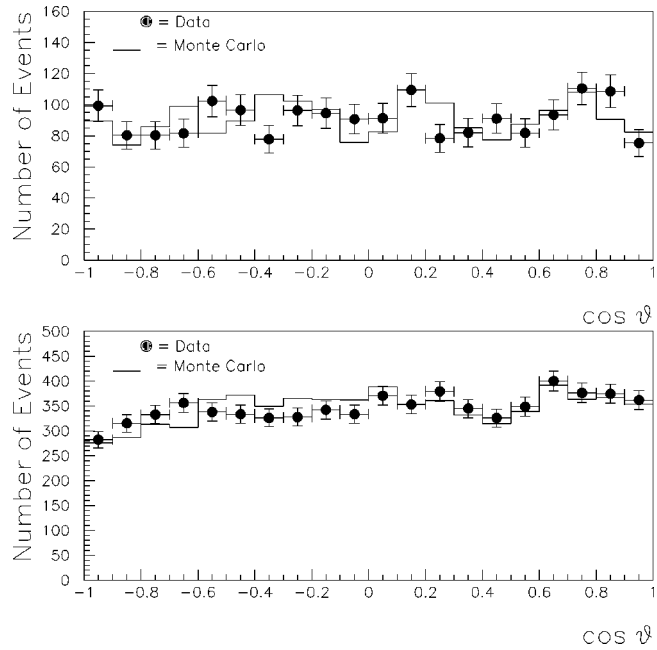

FIG. 11. The Monte Carlo ($\alpha_\Lambda\alpha_\Omega=-0.015$) fit to the cos θ distribution for $\overline{\Omega}^+$ (top) and Ω^- (bottom). The Monte Carlo distributions correspond to the measured $\alpha_\Lambda\alpha_\Omega$ yielding the best fits. The $\chi^2/19N_{DF}$ of the fits is 1.74 for $\overline{\Omega}^+$ and 1.49 for Ω^-.

We obtained the $\alpha_\Lambda\alpha_\Omega$ which gave the best match between data and Monte Carlo spectra by minimizing this function. The best fit for $\overline{\Omega}^+$ yielded $\alpha_{\overline{\Lambda}}\alpha_{\overline{\Omega}}=-0.011\pm0.041$, and the corresponding result for Ω^- was $\alpha_\Lambda\alpha_\Omega=-0.018\pm0.021$. The uncertainties are statistical only. Figure 11 shows the result of the final fits for $\overline{\Omega}^+$ ($\chi^2/N_{DF}=1.74$) and Ω^- ($\chi^2/N_{DF}=1.49$), which were obtained with sample No. 9 (see Table V).

To estimate the systematic uncertainty due to our event reconstruction algorithm, we first calculated the difference between the generated and reconstructed cos θ with Monte Carlo events. Then, we introduced a small, random offset to the cos θ calculation in the generated Monte Carlo events and again calculated the difference between the generated and reconstructed cos θ. The size of the offset was chosen to

TABLE V. Decay parameter measurements.

Sample No.	$\alpha_{\overline{\Lambda}}\alpha_{\overline{\Omega}}$	$\alpha_\Lambda\alpha_\Omega$
1	-0.017 ± 0.041	-0.006 ± 0.021
2	-0.001 ± 0.041	-0.010 ± 0.021
3	-0.020 ± 0.041	-0.015 ± 0.021
4	-0.009 ± 0.042	-0.024 ± 0.021
5	-0.013 ± 0.041	-0.007 ± 0.021
6	-0.005 ± 0.041	-0.018 ± 0.021
7	-0.015 ± 0.041	-0.016 ± 0.021
8	-0.021 ± 0.041	-0.004 ± 0.021
9	-0.011 ± 0.041	-0.018 ± 0.021
10	-0.014 ± 0.041	$+0.006\pm0.021$

TABLE VI. Systematic uncertainties for decay parameter measurements.

Systematic	$\alpha_{\bar{\Lambda}}\alpha_{\bar{\Omega}}$	$\alpha_{\Lambda}\alpha_{\Omega}$
Event selection	0.020	0.015
M2 field	0.003	0.005
Bin width	0.008	0.010
MC statistics	0.007	0.005
Reconstruction algorithm	0.010	0.005
MC sample	0.006	0.008
Acceptance	0.009	0.002
α_{Λ}	0.005	0.004

be consistent with the momentum resolution of the spectrometer. We estimated this systematic uncertainty by comparing the distributions (with and without the offset) of the difference between generated and reconstructed cos θ. No significant systematic effect due to the event reconstruction algorithm was observed.

The acceptance is momentum dependent. We estimated the uncertainty in $\alpha_{\Lambda}\alpha_{\Omega}$ due to our uncertainty in the momentum spectrum by studying various Ω Monte Carlo samples generated with slightly different momentum spectra. The fit results were not significantly different from the results obtained with the nominal momentum spectrum. Thus, this systematic uncertainty is small.

The effect of the uncertainty in the α_{Λ} parameter on the α_{Ω} measurement was also studied. Monte Carlo events were generated with an α_{Λ} offset by one standard deviation from its accepted value [1], and the fits were redone using these Monte Carlo events. The systematic effect due to the uncertainty in the α_{Λ} parameter was small when compared to other sources of systematic uncertainties.

The calculation of the other systematic uncertainties for the decay parameter analyses was similar to the lifetime analysis. The major sources of systematic uncertainties for the decay parameter analyses are listed in Table VI. The systematic uncertainties were estimated with Monte Carlo sample No. 3 (see Table V).

The final result for $\bar{\Omega}^+$ is $\alpha_{\bar{\Lambda}}\alpha_{\bar{\Omega}}=-0.011\pm0.041(\text{stat})\pm0.028(\text{syst})$, and the corresponding result for Ω^- is $\alpha_{\Lambda}\alpha_\Omega=-0.018\pm0.021(\text{stat})\pm0.022(\text{syst})$. By adding the statistical and systematic uncertainties in quadrature, we obtain $\alpha_\bar{\Lambda}\alpha_{\bar{\Omega}}=-0.011\pm0.050$ and $\alpha_{\Lambda}\alpha_{\Omega}=-0.018\pm0.030$. These can be divided by $\alpha_{\Lambda}=-\alpha_{\bar{\Lambda}}=0.642\pm0.013$ [1] to obtain

$$\alpha_{\bar{\Omega}}=0.017\pm0.077,$$

$$\alpha_{\Omega}=-0.028\pm0.047.$$

C. Mass difference

The normalized mass difference between the $\bar{\Omega}^+$ and Ω^- can be expressed as

$$\frac{\Delta M_{\Omega}}{M_{\Omega}}=\frac{|M_{\bar{\Omega}^+}-M_{\Omega^-}|}{M_{\text{average}}},$$

where $M_{\bar{\Omega}^+}$ and M_{Ω^-} are determined from the fit to their mass spectra and M_{average} is the weighted average of $M_{\bar{\Omega}^+}$ and M_{Ω^-}. We concentrate on the mass difference measurement rather than absolute mass measurements since the former is less sensitive to the uncertainty in the mass scale.

In order to obtain a precise measurement of the mass difference between the $\bar{\Omega}^+$ and Ω^-, we loosen the selection cuts to obtain higher statistics samples. The selection cuts for this analysis are similar to the lifetime and decay analyses selection except for the following:

(i) The reconstructed $M_{p\pi}$ was restricted to the range $1.0757<M_{p\pi}<1.1557$ GeV/c^2.

(ii) The angular cuts [see Sec. IV, paragraphs (h) and (i)] were removed.

(iii) The reconstructed $M_{\Lambda K}$ was restricted to the range $1.650<M_{\Lambda K}<1.700$ GeV/c^2.

(iv) The $\bar{\Omega}^+$ momentum spectrum was softer than the Ω^- momentum spectrum. This caused the spatial distribution of the $\bar{\Omega}^+$ and Ω^- decay daughter particles to be different, which directly affected the aperture cut (see below). Therefore, we ''matched'' the two momentum spectra by randomly selecting Ω^- events so that the Ω^- momentum spectrum matched the $\bar{\Omega}^+$ momentum spectrum. After the spectrum shape was ''matched,'' the Ω^- sample was about 2.6 times larger than the $\bar{\Omega}^+$ sample.

(v) The extrapolation of the three tracks from the candidate event to the downstream aperture of M2 was required to be within a rectangular-shaped area (50×20 cm^2) around the central region of the downstream aperture. This was motivated by the fact that the momentum measurement of the daughter tracks was well determined in that region, where the magnetic field was nearly uniform (see Fig. 12).

After these cuts, the ΛK invariant mass distributions were fit with the sum of a Gaussian and a linear function. This choice of fitting function was determined from the Monte Carlo simulation of the signal and backgrounds. The mass was determined from the mean of the Gaussian part of the fit. The background, which was estimated from the linear part of the fit, was 11.29% (9.19%) for $\bar{\Omega}^+$ (Ω^-). The background was higher here than in Sec. IV because we have eliminated some selection criteria that could bias the mass measurement. The standard deviation of the reconstructed mass was $\sigma\simeq2.3$ MeV/c^2, which agreed with the predicted mass resolution for these final states. Based on these fits, we estimated the number of Ω candidates by integrating the area under the Gaussian peak. We obtained 2607 ± 17 $\bar{\Omega}^+$ and 6323 ± 24 Ω^- candidate events, which included the uncertainty in the background under the Gaussian peak.

The fits yielded $M_{\bar{\Omega}^+}=1671.983\pm0.067$ MeV/c^2 and $M_{\Omega^-}=1671.959\pm0.038$ MeV/c^2, where the uncertainties are statistical only. This leads to $\Delta M_{\Omega}/M_{\Omega}=(1.44\pm4.59)\times10^{-5}$, where the uncertainty, again, is statistical only.

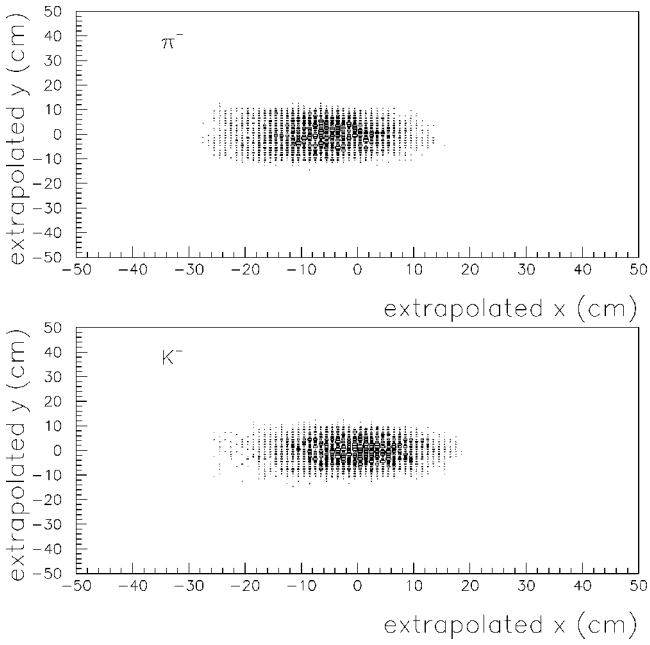

FIG. 12. Extrapolation of the π^- (top) and K^- (bottom) tracks at the M2 downstream aperture for $\Omega^- \to \Lambda K^-$ before applying the aperture cut.

Figure 13 shows the results of the final fits superimposed on the mass distributions for $\overline{\Omega}^+$ ($\chi^2/N_{DF}=1.70$) and Ω^- ($\chi^2/N_{DF}=1.46$).

Fluctuations in the magnetic field of M2 affect this measurement, since it causes the reconstruction code to miscalculate track momenta and reconstructed Ω mass. We estimated this systematic uncertainty by varying the nominal M2 magnetic field in the Monte Carlo simulation by 0.25% (see Sec. V A). The uncertainty due to magnetic field changes in M2 was small when compared to other major sources of systematic uncertainties.

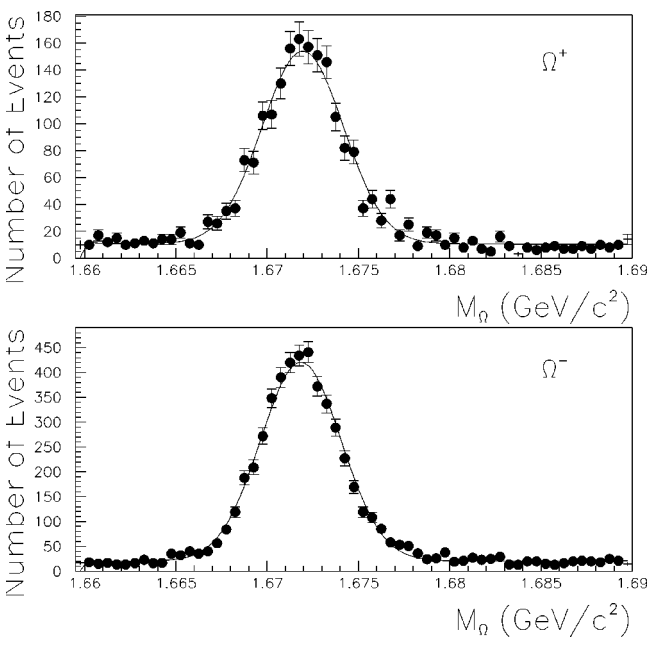

FIG. 13. Comparison of mass distributions for $\overline{\Omega}^+$ (top) and Ω^- (bottom) with fits superimposed. The $\chi^2/56N_{DF}$ of the fits is 1.70 for $\overline{\Omega}^+$ and 1.46 for Ω^-.

We studied the stability of the mass fits with respect to the size of the M2 aperture by varying the aperture cut. The mass fits varied by less than 0.3 standard deviations in the region where the magnetic field was measured to be nearly uniform.

We also studied the effect of the Λ-K and p-π opening angles $\theta_{\Lambda K}$ and $\theta_{p\pi}$ on the mass fits. An accurate determination of $\theta_{\Lambda K}$ and $\theta_{p\pi}$ depends on our understanding of the spectrometer alignment and reconstruction code. To estimate the systematic uncertainty in the mass difference analysis arising from the uncertainty in the determination of the opening angles, the data sample first was divided into three mutually exclusive regions with respect to $\theta_{p\pi}$ ($0° < \theta_{p\pi} \leqslant 0.133°$, $0.133° < \theta_{p\pi} \leqslant 0.187°$, and $\theta_{p\pi} > 0.187°$) with roughly the same number of events in each region. The fits were redone for both positive and negative data, and the corresponding Ω mass difference was recalculated for each region. The data were also divided into three mutually exclusive regions with respect to $\theta_{\Lambda K}$ ($0° < \theta_{\Lambda K} \leqslant 0.12°$, $0.12° < \theta_{\Lambda K} \leqslant 0.16°$, and $\theta_{\Lambda K} > 0.16°$), and a similar procedure was used to analyze each region. We estimated the systematic uncertainty due to $\theta_{p\pi}$ and $\theta_{\Lambda K}$ by comparing the mass difference for each region with the nominal mass difference (obtained from the full samples). The systematic uncertainty due to $\theta_{p\pi}$ and $\theta_{\Lambda K}$ was small when compared to other sources of systematic uncertainties.

The fitting method was checked by generating and fitting Monte Carlo samples with known input M_Ω, to ensure that the fit results were consistent with input values. Three independent Monte Carlo samples were generated with different input Ω mass (1637.0 MeV/c^2, 1672.45 MeV/c^2, and 1707.0 MeV/c^2). Each sample contained 100 000 events. The magnetic field of M2 was fixed at the nominal value ($p_T = 1.54$ GeV/c). The upstream and downstream apertures of M2 were also fixed at their nominal values (see Sec. II). The Monte Carlo events were generated with a momentum spectrum similar to that of the data at the exit of M1 and were subjected to the same reconstruction selection cuts as the data. The systematic uncertainty in the mass difference measurement due to the fitting method was small when compared to the statistical uncertainty.

The bin widths were doubled to check the sensitivity of the analysis to the binning method and the mass resolution of the spectrometer. The systematic uncertainty in the mass difference measurement due to the bin width was negligible.

We also checked if the code reconstructs $\overline{\Omega}^+$ and Ω^- events differently. We generated $\overline{\Omega}^+$ and Ω^- Monte Carlo events, with both masses fixed at the accepted value ($M_\Omega = 1672.45$ MeV/c^2) [1]. The events were processed through the same reconstruction code, and we then calculated the Ω mass difference using values for $M_{\overline{\Omega}^+}$ and M_{Ω^-} from Monte Carlo events and compared with the Ω mass difference from data. This turned out to be the dominant source of systematic uncertainty.

TABLE VII. Systematic uncertainties for mass difference measurement.

Systematic	$\Delta M_\Omega/M_\Omega$ $(\times 10^{-5})$
M2 field	0.598
Aperture	2.677
$\theta_{p\pi}$ and $\theta_{\Lambda K}$	1.995
Fitting method	2.847
Bin width	1.005
Monte Carlo	3.618
Momentum	2.991
Mass scale	0.059

The systematic uncertainty in the mass ratio due to the uncertainty in momentum was estimated by dividing each data sample into three bins with roughly the same number of events in each bin and redoing the analysis for each bin, as in the lifetime analysis. The mass fits varied by less than 0.5 standard deviations, which indicates that the momentum ''matching'' procedure helped to smooth out the differences in the mass measurements due to differences in momentum spectra between $\overline{\Omega}^+$ and Ω^-.

A good understanding of the mass scale is necessary to obtain a reliable mass measurement. We estimated the uncertainty in the mass scale by comparing the measured Ξ and Ω masses with the accepted values [1]. The difference is approximately 0.860 MeV/c^2. The measurement of the ratio $\Delta M_\Omega/M_\Omega$ is less sensitive to the uncertainty in the mass scale than absolute mass measurements. We found the systematic uncertainty due to the mass scale to be small when compared to other sources of systematic uncertainties for the mass difference analysis. The major systematic uncertainties are summarized in Table VII.

The final result for the normalized mass difference is

$$\frac{\Delta M_\Omega}{M_\Omega}=(1.44\pm 7.98)\times 10^{-5},$$

where the statistical and systematic uncertainties were added in quadrature.

VI. SUMMARY

A sample of 1823 $\overline{\Omega}^+$ and 6953 Ω^- events has been analyzed to produce various results (see Table VIII). The $\overline{\Omega}^+$ lifetime measurement yielded

TABLE VIII. Summary of analysis results.

Measurement	$\overline{\Omega}^+$	Ω^-
τ $(\times 10^{-10}$ s)	0.823 ± 0.038	0.817 ± 0.022
α_Ω	0.017 ± 0.077	-0.028 ± 0.047
$\Delta M_\Omega/M_\Omega$ $(\times 10^{-5})$	1.44 ± 7.98	

$$\tau_{\overline{\Omega}}=(0.823\pm 0.038)\times 10^{-10}\ \text{s},$$

and the decay parameter measurement yielded

$$\alpha_{\overline{\Omega}}=0.017\pm 0.077.$$

These lifetime and α_Ω measurements for the $\overline{\Omega}^+$ hyperon are the first such measurements in the literature [1]. The corresponding values for Ω^- were

$$\tau_\Omega=(0.817\pm 0.022)\times 10^{-10}\ \text{s},$$

and

$$\alpha_\Omega=-0.028\pm 0.047,$$

in good agreement with previously published results [8]. The normalized mass difference between $\overline{\Omega}^+$ and Ω^- was

$$\Delta M_\Omega/M_\Omega=(1.44\pm 7.98)\times 10^{-5},$$

which should be compared to the previous world average $\Delta M_\Omega/M_\Omega$ measurement of $(0\pm 5)\times 10^{-4}$ [9].

ACKNOWLEDGMENTS

We gratefully acknowledge the assistance of the staff at Fermilab. This work was supported in part by the U.S. Department of Energy, the U.S. National Science Foundation, and the National Science Council of the Republic of China.

[1] Particle Data Group, R. M. Barnett *et al.*, Phys. Rev. D **54**, 1 (1996).
[2] T. D. Lee and C. N. Yang, Phys. Rev. **108**, 1645 (1957).
[3] J. Finjord, Phys. Lett. **76B**, 116 (1978).
[4] R. Carosi *et al.*, Phys. Lett. B **237**, 303 (1990).
[5] B. Schwingenheuer *et al.*, Phys. Rev. Lett. **74**, 4376 (1995).
[6] P. M. Ho *et al.*, Phys. Rev. D **44**, 3402 (1991).
[7] H. T. Diehl, Ph.D. thesis, Department of Physics and Astronomy, Rutgers University, 1990.
[8] M. Bourquin *et al.*, Nucl. Phys. **B241**, 1 (1984).
[9] E. P. Hartouni *et al.*, Phys. Rev. Lett. **54**, 628 (1985).